A Testbed for The Rapid Prototyping of Tendon Driven Dexterous Fingers with Highly Redundant Sensing

David M. McDougall, Anthony J. Barcio, Gray C. Thomas, Robert O. Ambrose

***Abstract*— Inspired by the Robonaut 2 hand architecture and force sensing capabilities. A tendon-driven dexterous robotic finger testbed with Bowden tube routing is presented. In addition to the strain gauge tension measurement from R2, the testbed incorporates a planar rotatory spring for high-fidelity cable tension control. This paper discusses details and design considerations for the testbed, including Bowden tube routing and actuator architecture.**

I. INTRODUCTION

Dexterous robotic hands have emerged from the desire for robotic systems to interact with interfaces designed for humans [1–4]. These interfaces are often difficult for traditional robot end-effectors to use, since humans possess and exploit numerous well-controlled hand degrees of freedom with comparatively advanced manipulation capacity. However, practically achieving this goal remains a design and control challenge for high degree of freedom tendon-driven robot hands, in part because complex tendon-routing systems introduce friction that hinders the prediction and control of the internal forces of multi-contact. This work specifically builds upon dexterous tendon-driven hands with force-feedback sensors and bowden tube tendon routing. Specifically, this testbed is meant to innovate dexterous hands based upon the Valkyrie hand [5] and Robonaut II hand [6] architectures which face the additional difficulty of overcoming the friction in a Bowden cable. The Robonaut hand sought to measure the cable force through sensing the compression in the Bowden tube with a series of strain gauges, however these sensors were noisy and required temperature compensation.

To learn from and improve upon these systems, we propose a testbed with both Bowden tube termination compression sensing and series-elastic actuation (SEA) to provide complete friction sensing capabilities to rapidly test and improve tendon-driven robotic fingers. Our modular design allows for rapidly developing systems because interoperability between different modules allows for parallel iteration of different components. This is achieved through standardized mounting interfaces for each subsystem and will enable researchers to rapidly swap and evaluate new versions of each module without requiring redesigns of other modules. This paper presents a detailed overview of the testbed design with respect to the finger architecture, Bowden tube termination, and actuator design.

**Research supported by the Texas A&M Chancellor's Research Initiative and the Texas Governor's University Research Initiative.

Authors are with Texas A&M University Robotics and Automation Design (RAD) Lab

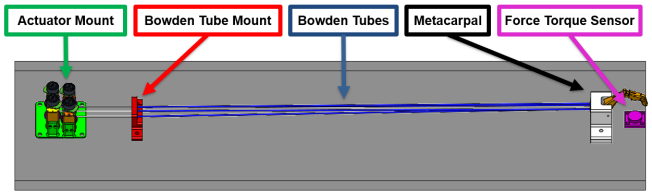

Fig. 1. Top view of the Modular Finger Testbed with important modules labeled

II. TESTBED DESIGN

The testbed consists of four modules: actuators, Bowden tube assembly, metacarpal, and force-torque sensor. The metacarpal is the mounting point for the finger and the termination of the Bowden tubes. The Bowden tubes route the tendons from the actuators to the finger and serve both to emulate the architecture of a robotic hand [5, 6] and alleviate the change in tendon arrangement between the actuators and the metacarpal. A force torque sensor is mounted in front of the metacarpal to characterize the strength, contact forces, and control of the specific finger being tested. The actuators are mounted to a common adapter plate to group the tendons as tightly as possible. This is maintained throughout the tendon routing to decrease friction losses. A large distance separates the metacarpal from the Bowden tube mount to decrease the curvature in the Bowden tubes. Figure 1 shows the design of the testbed.

For the purposes of this paper, a secondary digit [6] with 3 degrees of freedom is used to present a starting point for this class of testbed. To control both flexion and extension, four actuators are used. Two opposed actuators control the distal tendon, while the medial and proximal joints are only actuated in flexion.

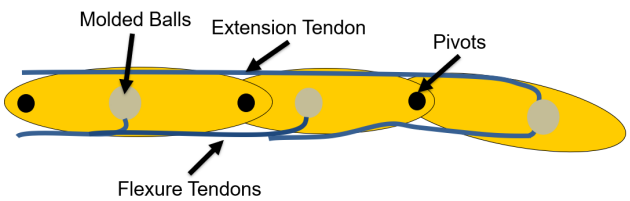

Fig. 2. A simplified version of the proposed finger that displays the routing of the tendons

III. Finger Design

The modularity of the proposed testbed allows any tendon-driven finger to be tested by adapting the mounting mechanism to fit the metacarpal. The underactuated 3-degree-of-freedom finger from DexHand is used here as a representative model [4]. This paper proposes certain design innovations for a rapidly manufactured finger prototype, the CAD of which is not available for publication at this time.

The proposed finger is manufactured by 3D printing each joint in two pieces and bolting them together after the tendons are attached. The tendons are manufactured from high-strength Kevlar line and attach to the finger by molding a small plastic ball directly around a knot in each tendon and placing the balls inside a spherical cavity in each joint. These attachments will be referred to as the termination of the tendon. These balls transmit the tendon tension into each link to actuate the finger joint. This termination style allows for efficient force transmission while reducing stress concentrations in the tendon filament.

The three flexor tendons extend along the bottom of the finger with the distal flexor tendon sharing a ball with the extensor tendon. Figure 2 is a simplified version of the proposed finger design that shows the routing scheme for the tendons. The tendons are routed through the finger with the flexor tendons sharing a pathway traveling below the finger, and the extensor tendon following a channel in the top of the finger. At full flexion, the lower channel forms a large-diameter, constant-curvature arc, increasing the strength of the finger in this condition; the analysis presented in Section V-B shows that the strength increases with larger pulley diameter at the finger joints. This channel geometry also reduces stress concentrations in the tendon.

IV. Bowden Tube and Metacarpal Design

The Bowden tubes provide routing from the motors to the base of the metacarpal for the tendons, and increase the number of actuated degrees of freedom available by eliminating the space required for pulleys. This applies to both the testbed itself and a dexterous robotic hand. However, Bowden tubes introduce friction losses between the motor and the metacarpal, which introduce uncertainty in tension-based force sensing and control. The Robonaut II system, shown in Fig. 3, mitigates this uncertainty by placing a tension sensor at the end of the Bowden tube and reports measurement of the tension in each tendon within a 10%-15% error [6]. Section V-A discusses proposed improvements on this method. The testbed follows this design approach and routes the Bowden tubes from the actuators through the metacarpal. The modular design of the testbed allows for different Bowden tube lengths and geometries to be evaluated for their respective frictional losses.

Figure 4 shows the attachment points for the Bowden tubes to the metacarpal in the proposed testbed. The tendons travel freely through the interior of the metacarpal toward their connection points on the finger after exiting the Bowden tubes.

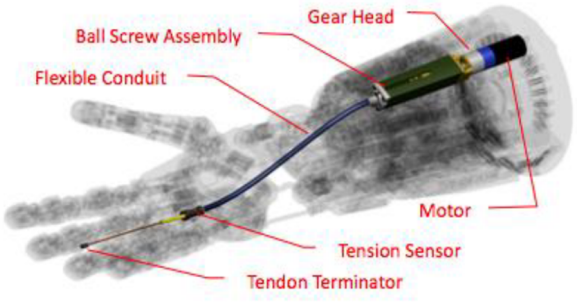

Fig. 3. Actuator and Bowden tube routing for Robonaut II [6]

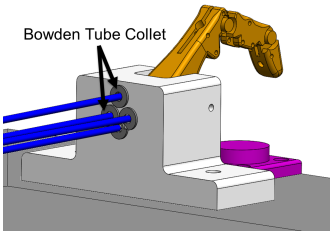

Fig. 4. Local view of the Bowden tubes terminating in the metacarpal

V. Actuator Design

A. Design and Philosophy

Robonauts I and II utilized linear actuators [2] and BLDC motors with lead-screw reductions [6] respectively to actuate finger tendons in the forearm. To minimize volume, actuators for this testbed use a BLDC motor with a miniature strain wave reducer similar to the Valkyrie robotic hand [5]. A pulley attached to the strain wave reducer terminates the tendon similarly to the method outlined in Section III. This design architecture additionally allows for a planar rotary spring (PRS) to sense tendon tension and implement SEA control of the finger. This choice is an intended improvement over previous hands which featured force sensitivity through strain gauges and barometric pressure sensing, but not full SEA control [2, 5, 6]. Additionally, the introduction of a PRS for tension sensing provides a non-temperature sensitive method of force measurement. The overall design architecture can be seen in Fig. 6.

By adding designed-in compliance at the actuator in addition to finger joint and Bowden termination force sensing, losses from different sources in a robotic hand can now be measured directly and separately by source: the gear train, the Bowden tube through the wrist, and the finger joints themselves. This would allow for the detection of wear in certain components, such as the Bowden tube, and could allow a robotic hand to perform autonomous fault detection for issues like this.

Figure 5 shows a notionally appropriate spring profile following the design style of PRS used in larger actuators in Robonaut II and Valkyrie [1, 7]. This particular design was generated in Abaqus FEA out of AL7075 to have an appropriate stiffness and torque capacity based on the actuator sizing in Section V-B. Alternative design strategies

Fig. 5. Possible PRS profile

for the PRS could involve a two-part spring architecture proposed by Bons et. al [8]. There is additionally significant forward work to be done to develop compact progressive springs for this application, as a finger whose actuators are equipped with progressive springs could vary its stiffness simply by contracting each actuator equally, thereby equally preloading each tendon and its corresponding PRS, increasing the stiffness of the digit without changing its pose.

The structure of the actuator is designed with forearm integration in mind, featuring flanges meant to bolt into the outer structure of the forearm. An annotated actuator design is presented in Fig. 7.

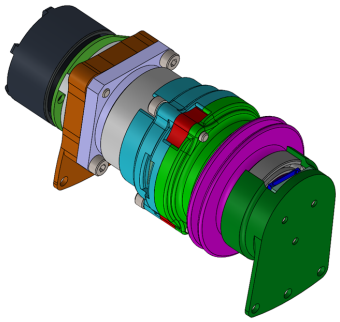

Fig. 6. Isometric view of actuator module CAD.

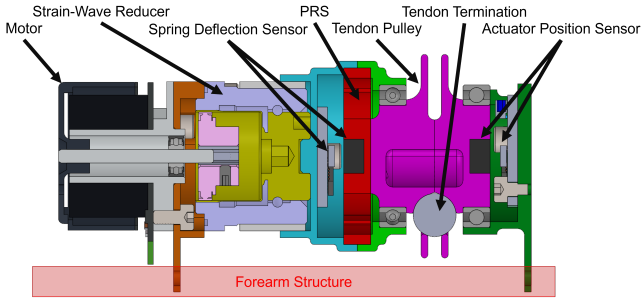

Fig. 7. Annotated cross section of a finger joint actuator module

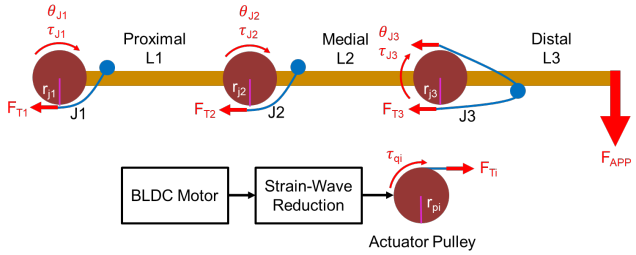

Fig. 8. Kinematic diagram of a proposed finger module

B. Kinematic Analysis

To size the actuators, a kinematic analysis of the initial finger design was performed to evaluate actuator effort under a specified tip load at full extension. Full extension is the worst-case scenario in terms of strength for the finger architecture as defined in Section III. The pulley radius for each actuator was selected so that the overall mechanical advantage from each BLDC motor to its respective finger joint (and therefore the effort required at each actuator module) is equivalent in the full-extension regime. The strain wave reduction ratio was kept constant to reduce the unique part count.

This design philosophy for actuators is part of the testbed's overall commitment to modularity, allowing the commercial-off-the-shelf (COTS) components of each actuator to remain invariant over the entire finger. This allows drop-in replacement of any actuator module within the testbed. The reliance on COTS parts also decreases the cost of development. The next step in this analysis involves generalization across every finger in a hand, allowing for easy drop-in replacement of any actuator module within the entire forearm.

$$[\tau_q] = J_{act} J_{tens}^{-1} J^T [F_{APP}]$$

where

$$J_{act} = \begin{bmatrix} r_{p1} & 0 & 0 \\ 0 & r_{p2} & 0 \\ 0 & 0 & r_{p3} \end{bmatrix} \quad (1)$$

and

$$J_{tens} = \begin{bmatrix} r_{j1} & r_{j1} & r_{j1} \\ 0 & r_{j2} & r_{j2} \\ 0 & 0 & r_{j3} \end{bmatrix}$$

Equation 1 defines the transform from loads in cartesian space (F_{APP}) to loads in actuator space (τ_q), according to the dynamics shown in Figure 8. For the purpose of this analysis, the actuator used for extension is disregarded. J_{tens} represents the Jacobian between loads on each finger joint (torques τ_{Ji} in Fig. 8) and tendon tensions (F_{Ti}). J represents the Jacobian between loads on each finger joint and loads in cartesian space. The general form of the Jacobian, dependent on joint angle (θ), has too many terms to be presented here, but simplifies to Equation 2 for the full extension ($\theta = [0, 0, 0]^T$) case:

$$J = \begin{bmatrix} 0 & 0 & 0 \\ L1 + L2 + L3 & L2 + L3 & L3 \\ 0 & 0 & 0 \end{bmatrix} \quad (2)$$

This represents a system of linear equations for which pulley radii r_{p1}, r_{p2}, r_{p3} can easily be solved such that all elements of τ_q are equal. r_{p4}, corresponding to the extensor tendon, can be made equal to r_{p3}. This particular approach focuses on designing an actuator that envelopes all load cases while minimizing the unique part count and not "wasting" any actuator capability. There is significant forward work to be done to generalize this analysis across different finger poses, which would involve a unique value for r_{p4}.

C. Final Design and Component Selection

A Maxon ECXFL22L (ECX Flat series, ⌀22mm) motor and Harmonic Drive CSF-5-2XH (⌀30mm) reduction were selected for the testbed based on the analysis in Section V-B. These parts meet the maximum effort requirements while minimizing the overall radius and stackup length of the actuators. No actuator exceeds an envelope of 68mm lg. x 30mm ⌀, disregarding mounting flanges. With efficient packing, this results in a theoretical forearm design which fits 24 actuators into an envelope of 292mm lg x 105mm ⌀, with a 32mm ⌀thru-bore to contain Bowden tubes and cable harness. A space claim model of the forearm with the proposed actuator packing is shown in Figure 9.

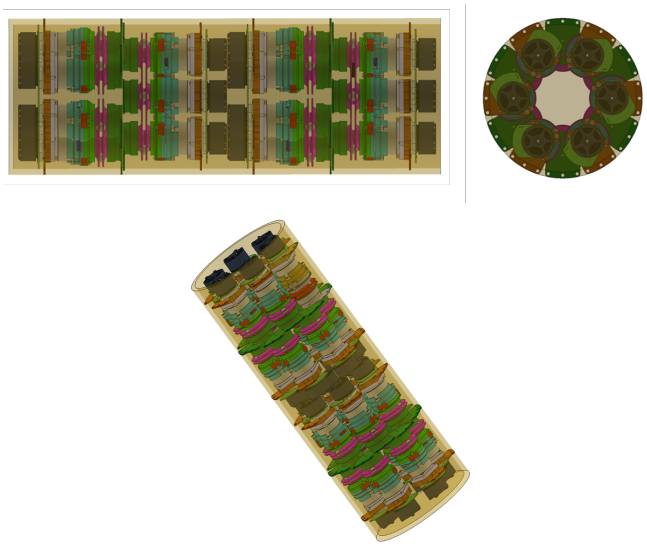

Fig. 9. Various views of a possible forearm arrangement

VI. Conclusion

Dexterous robotic hands are increasingly important in a world where robots need to interact with systems built for humans. Modular testbeds with capabilities for tension and friction sensing will aid in the development and characterization of new dexterous fingers with increased sensitivity. These advancements contribute to rapid iteration and innovation through the decoupling of subsystems, enhancing the plug-and-play design style, and improving the characterization of tendon behavior. Looking forward, this will allow for the testing of innovations on existing hand architectures such as compact progressive springs for digit stiffness adjustment, effort-equalizing pulley design for pose-independent grip strength, and redundant force sensing for high-fidelity friction measurement and compensation. Once this testbed has been built and characterized, incorporating these advancements into a full robotic hand becomes a packaging problem.

References

[1] M.A. Diftler et al. "Robonaut 2 - The first humanoid robot in space". In: *2011 IEEE International Conference on Robotics and Automation*. 2011, pp. 2178–2183. DOI: 10.1109/ICRA.2011.5979830.

[2] C. S. Lovchik, H. A. Aldridge, and M. A. Diftler. "Design of the NASA Robonaut Hand". In: vol. Dynamic Systems and Control. ASME International Mechanical Engineering Congress and Exposition. Nov. 1999, pp. 823–830. DOI: 10.1115/IMECE1999-0113. eprint: https://asmedigitalcollection.asme.org/IMECE/proceedings-pdf/IMECE99/16349/823/6812981/823_1_imece1999-0113.pdf. URL: https://doi.org/10.1115/IMECE1999-0113.

[3] J. Butterfass et al. "DLR-Hand II: next generation of a dextrous robot hand". In: *Proceedings 2001 ICRA. IEEE International Conference on Robotics and Automation (Cat. No.01CH37164)*. Vol. 1. 2001, 109–114 vol.1. DOI: 10.1109/ROBOT.2001.932538.

[4] Rob Knight and Trent Shumay. *DexHand - An Open Source Dexterous Humanoid Robot Hand*. URL: https://www.dexhand.org/ (visited on 04/14/2025).

[5] Nicolaus Radford et al. "Valkyrie: NASA's First bipedal humanoid robot". In: *Journal of Field Robotics* 32 (May 2015), pp. 397–419. DOI: 10.1002/rob.21560.

[6] L. B. Bridgwater et al. "The Robonaut 2 hand - designed to do work with tools". In: *2012 IEEE International Conference on Robotics and Automation*. 2012, pp. 3425–3430. DOI: 10.1109/ICRA.2012.6224772.

[7] Nicholas Paine et al. "Actuator Control for the NASA-JSC Valkyrie Humanoid Robot: A Decoupled Dynamics Approach for Torque Control of Series Elastic Robots". In: *Journal of Field Robotics* 32 (May 2015). DOI: 10.1002/rob.21556.

[8] Zachary Bons et al. "A Compact, Two-Part Torsion Spring Architecture". In: *2023 IEEE International Conference on Robotics and Automation (ICRA)*. 2023, pp. 7461–7467. DOI: 10.1109/ICRA48891.2023.10161174.